Smart Forestry

ORIGINAL RESEARCH

Open Access

https://doi.org/10.48130/smartfor-0026-0005

Smart Forestry **2026**, 1: e008

Multi-modal proximal sensing of structural and spectral traits for clonal selection of color-leaved tree seedlings

Ding Zhang[1#], Ling Chen[1#], Linyuan Li[1*], Qian Bai[1], Zhexiu Yu[2], Xiaohui Jiang[3], Jianying Liu[3] and Huaguo Huang[1]

[1] *State Key Laboratory to Efficient Production of Forest Resources, College of Forestry, Beijing Forestry University, Beijing 100083, China*
[2] *School of Soil and Water Conservation, Southwest Forestry University, Kunming 650224, China*
[3] *Hongyashan State-owned Forest Farm, Yixian 074200, China*
[#] Authors contributed equally: Ding Zhang, Ling Chen
[*] Correspondence: lilinyuan@bjfu.edu.cn (Li L)

Abstract

Early selection is of great significance for accelerating the breeding of color-leaved tree species. However, traditional phenotypic assessment lacks sufficient characterization of three-dimensional structure and color traits, both of which are particularly important for color-leaved tree species. Moreover, few studies have applied proximal sensing techniques to the breeding and selection of color-leaved tree species. In this study, we integrated unmanned aerial vehicle (UAV) imagery and terrestrial laser scanning (TLS) point cloud to characterize a suite of structural traits (i.e., physiological, morphological, and architectural complexity traits) and spectral traits (i.e., vegetation indices) in clonal seedlings from 13 provenances. We analyzed the correlations among those phenotypic traits and demonstrated their complementarity in characterizing 3D structure and coloration. Phenotypic variation was evaluated using principal component analysis (PCA), which exhibited the contribution of each trait and yielded composite scores ranging from −1.26 to 1.57. Analysis of variance (ANOVA) followed by Tukey's honestly significant difference (HSD) test were also applied, further confirming the significant differences among provenances. Finally, all clonal seedlings were grouped into four distinct types of clusters using K-means clustering based on all phenotypic traits, with each cluster exhibiting characteristics suitable for the target application. This study demonstrates the merit of multi-modal proximal sensing techniques for phenotyping identification and clonal selection of color-leaved tree seedlings.

Citation: Zhang D, Chen L, Li L, Bai Q, Yu Z, et al. 2026. Multi-modal proximal sensing of structural and spectral traits for clonal selection of color-leaved tree seedlings. *Smart Forestry* 1: e008 https://doi.org/10.48130/smartfor-0026-0005

Introduction

Color-leaved trees, owing to their diversity in forms and foliage color play an important role in urban landscape design[1]. *Pistacia chinensis (P. chinensis)*, a deciduous tree species endemic to China, exhibits strong ecological adaptability and is extensively used in ornamental horticulture programmes[2,3]. The phenotypic traits of *P. chinensis* are significantly influenced by various factors such as genetics and the environment, leading to noticeable differences among individuals[4]. Given that the three-dimensional structural and spectral traits of *P. chinensis* are expressed during the seedling stage and persist through maturity, early clonal selection based on these traits represents an efficient strategy for identifying elite germplasm[5,6]. Traditional phenotypic identification methods rely heavily on labor-intensive manual measurements, which are primarily suited for two-dimensional (2D) growth traits such as crown width, plant height, and stem angle. However, these approaches are inadequate for capturing three-dimensional (3D) structural and spectral traits, which serve as more informative indicators for color-leaved tree selection.

High-throughput plant phenotyping (HTPP) technologies, particularly multi-modal proximal sensing, have emerged as powerful tools for trait identification, owing to their efficiency, scalability, and objectivity[7,8]. Among these, terrestrial laser scanning (TLS) and unmanned aerial vehicle (UAV) systems represent two prominent approaches increasingly employed in field-based plant phenotyping. TLS is particularly effective for capturing detailed three-dimensional structural traits, whereas UAV-based imagery enables efficient extraction of color-related and spectral traits[9–11]. Besides, UAV-based proximal sensing, known for its high mobility, wide coverage and efficient data acquisition, has been increasingly used for local-scale plant phenotyping and breeding research[12,13].

With its high-precision capability for 3D characterization, TLS enables the extraction of a broad range of phenotypic traits, extending from traditional 2D to complex 3D traits[14]. For instance, Jin et al. quantify individual-level maize traits (e.g., branch morphology, leaf inclination, and leaf length) by employing TLS point clouds in conjunction with a newly proposed Median-Normalized Vector Growth (MNVG) algorithm[15]. Zhu et al. monitored the canopy-level dynamics of wheat structural traits using backpack LiDAR and established correlations between structural traits and yield[16]. Gao et al. determined 11 elite *Ginkgo* individuals based on TLS-derived structural traits and demonstrated that TLS is a reliable tool for assessing tree phenotypes, and that elite individuals identified through TLS-based screening showed strong concordance with molecular-level validation[17]. Chen et al. proposed a set of novel morphological metrics, including projection compactness and volume compactness, to quantify plant form using point cloud data. Based on these metrics, sugar beets were classified into several morphological categories, and distinct patterns of structural variation were identified[18]. Liu et al. proposed a structural complexity metric, canopy entropy, to characterize the self-similarity of forest structures at both the stand and individual tree levels. However, the application of TLS to colored-leaf tree seedlings remains challenging due to their small size and intricate branching architecture, which complicate accurate trait extraction at the plant level[19]. Moreover, TLS alone is incapable of capturing foliar coloration, a critical phenotypic trait for colored-leaf germplasm.

By equipping UAVs with hyperspectral/multispectral sensors, researchers can rapidly obtain spectral vegetation indices to assess

plant physiological status and leaf pigment variation. Bhandari et al. employed UAV multispectral imagery to assess the extent of leaf damage caused by disease in winter wheat. The analysis revealed significant differences in vegetation indices among different severity levels[20]. Kerkech et al. showed that vegetation indices such as Excess Green (ExG), Excess Red (ExR), and ExGR effectively in capturing leaf color variations and can reflect leaf color. These indices, when combined with deep learning models, enable early detection[21]. These studies indicate that vegetation indices can capture changes in internal leaf pigments, thereby reflecting distinct physiological and biochemical states as well as observable leaf coloration. Although capable of capturing spectral variation, UAV-based imagery lacks the ability to retrieve the 3D-detailed structural information of plants. This limitation is particularly remarkable for color-leaved tree seedlings, where spectral imagery alone may overlook crucial morphological variations such as plant architecture and canopy structure, thereby undermining the accuracy and completeness of phenotypic identification.

Recent studies have shown that multi-modal proximal sensing can significantly enhance phenotypic identification capability, hence accelerate plant breeding. In a common-garden trial of 16 *Populus fremontii* populations, Sankey et al. fused UAV hyperspectral, thermal, and LiDAR data to reveal significant genotype-level differences in canopy height, leaf area, water, carbon, and nitrogen traits (producer's accuracies > 75%), enabling selection of climate-adapted and high-fitness genotypes[22]. Likewise, Gu et al. combined UAV LiDAR point clouds with multispectral imagery to derive novel 3D photosynthetic traits (e.g., CPn_P75th, CCC_P75th) that better predict wheat yields than traditional metrics, demonstrating applicability for cultivar selection[23]. These studies offer new avenues for multidimensional phenotypic characterization. Although such fusion strategies have been preliminarily applied in crop breeding, their application in forestry, particularly in color-leaved tree seedlings, remains scarce.

For color-leaved tree species, both color and structural characteristics are critical criteria in breeding selection. In particular, clonal seedlings of *P. chinensis* under field environments exhibit complex architectures, diverse coloration, and variable growth forms, posing significant challenges for comprehensive and accurate trait capture using any single-source proximal sensing method. To address this, the present study aims to develop a multi-modal proximal sensing framework capable of identifying a broad range of 2D and 3D structural and spectral traits, thereby facilitating precise clonal selection in *P. chinensis* seedlings. Specifically, this study addresses the following two questions: (1) Do the proposed structural and spectral traits sufficiently reflect the differences among seedlings? and (2) How can clonal seedlings with target traits be effectively selected?

Materials and methods

Study area

The experimental site is located in the Hongyashan state-owned forest farm, Yixian County, Hebei Province, China (115.56° E, 39.36° N) (Fig. 1). The region experiences a warm, temperate, semi-humid continental monsoon climate. Within the forest farm, a dedicated nursery has been established for the cultivation of *P. chinensis* seedlings. The terrain is flat and follows a ridge cultivation layout, covering an area of 80 m × 80 m. Ridges are spaced at 1 m intervals, with 2 m between individual plants. In spring 2023, a number of *P. chinensis* clonal seedlings were grafted using the cleft grafting method. All rootstocks originated from the same source and exhibited uniform and vigorous growth, thereby minimizing the influence of rootstock variation. The scions (referred to hereafter as clonal seedlings) were collected from different geographic provenances and individually labeled with identification cards. Visual inspection revealed notable variation among the clonal seedlings, including variations in terms of both structure and coloration traits. A representative 80 m × 30 m area within the nursery was selected as the experimental area, encompassing 13 provenances, including H2, J2, LGC, YJA, WJC, WA, SJ (from Hebei Province), BWL, MAS, SMF (from Henan Province), GL, YX (from Shandong Province), and GZZ (from Hubei Province). A total of 58 Pistacia chinensis clones were selected for this study. Each provenance included multiple clonal genotypes, with an example of clonal codes formatted as 'LGC-28', where the alphabetical prefix (e.g., 'LGC') represents the provenance origin, and the numerical suffix (e.g., '28') identifies the specific clonal lineage within that provenance

Data collection and pre-processing

An overview of the complete workflow, from data acquisition (TLS and UAV) to trait identification, is provided in Fig. 2.

Ground-based survey

The ground-based survey was conducted on November 13, 2024. Phenotypic traits of each *P. chinensis* clonal seedling within the selected area were measured (Table 1), including plant height (using a tape measure), scion diameter (using a vernier caliper), crown width (using a tape measure), mean angle of first-order branches (using a protractor), and compound leaf number (manual counting). Meanwhile, we also measured the leaf inclination angle of compound leaves using a self-developed laboratory instrument, LAMDA.

TLS data and preprocessing

The TLS data was acquired using a RIGEL-VZ1000 LiDAR system on November 12, 2024. Given the relatively large size of the selected nursery plot, a multi-single-scan strategy was adopted to ensure complete spatial coverage, resulting in a total of nine individual scans. The scanning configuration included a vertical field of view (FOV) of 30°–150°, a horizontal FOV of 0°–360°, and an angular resolution of 0.003°. Due to the small size of the seedlings, geometric inaccuracies arising from the coregistration of multiple scans often introduce non-negligible errors in subsequent analyses. To minimize such effects, for each seedling, only the point cloud from the scan with the highest point density was retained for further processing. Preprocessing of the TLS data was conducted in CloudCompare and included statistical outlier removal (SOR) for noise filtering, off-ground point classification using the Cloth Simulation Filter (CSF)[24], and height normalization of the off-ground point cloud. Individual seedling point clouds were segmented using LiDAR360 commercial software and subsequently verified and manually corrected through visual interpretation.

After the individual seedling segmentation, the point clouds were classified into leaf and woody components, with woody structures further subdivided into individual branches for trait analysis. To distinguish wood from leaves, a principal component analysis (PCA) was applied to each point and its local neighborhood to derive three eigenvalues (λ_1, λ_2, λ_3), representing local geometric characteristics. Woody points typically exhibit a linear distribution characterized by a dominant eigenvalue λ_1 that is markedly greater than λ_2 and λ_3[25]. Based on this principle, wood points were identified using an empirically defined threshold (Eq. [1]). The candidate wood points were subsequently clustered using the density-based

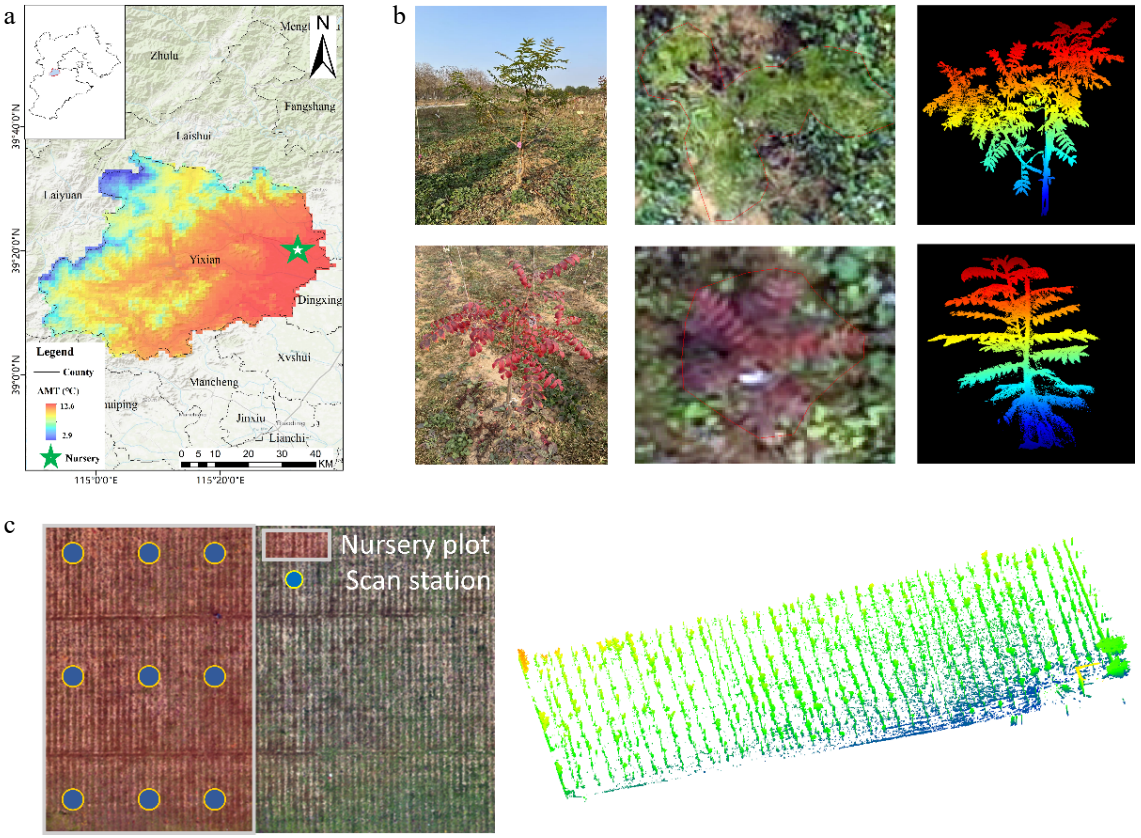

Fig. 1 (a) The experimental site of this study. (basemap source: Esri topographic map, generated using ArcGIS). (b) Example photos of cloned seedlings, UAV RGB orthophotos, and TLS point clouds. (c) The selected area in the *Pistacia chinensis* cloned seedling nursery, and the distribution of terrestrial laser scans (TLS), as well as single-station seedling TLS data.

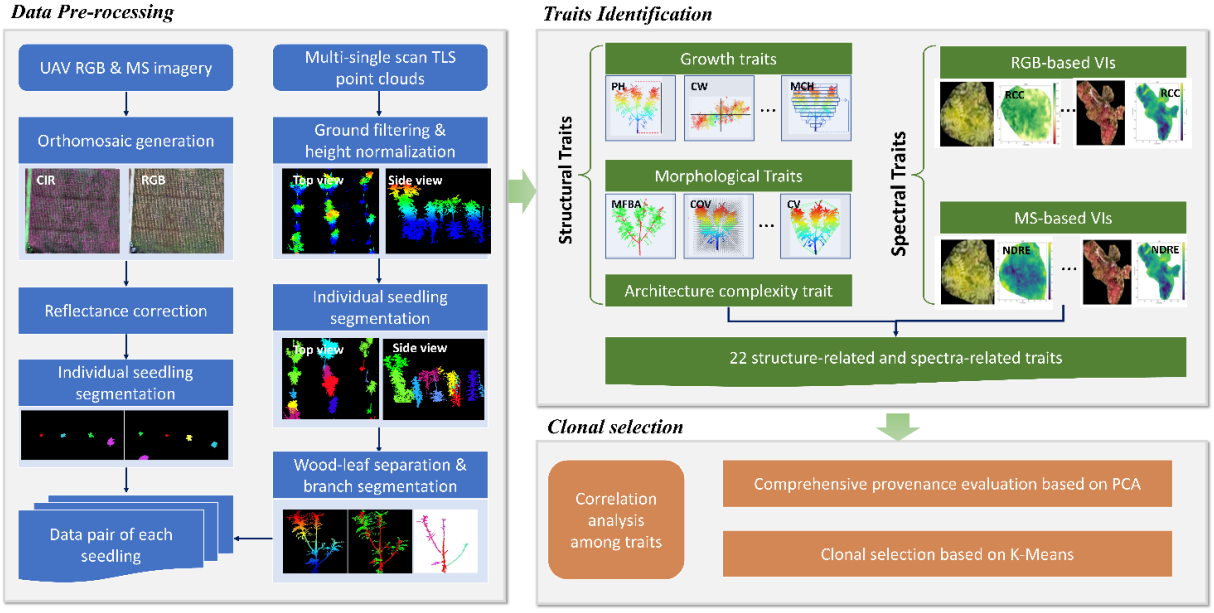

Fig. 2 Workflow diagram of the proposed multi-modal proximal sensing pipeline for seedling phenotyping. The workflow starts with TLS point cloud and UAV multispectral/RGB image acquisition, followed by stream-specific preprocessing, seedling-level processing, and finally outputs of structural- and spectral-trait tables for downstream analyses.

spatial clustering of applications with the noise (DBSCAN) algorithm[26,27]. Clusters containing more than a specific number of points and exceeding a spatial extent of 0.15 m were retained as woody structures.

$$\lambda 1 > 1.2 \times \lambda 2 > 1.32 \times \lambda 3, \quad (1)$$

To further differentiate the main stem from first-order branches, a Hierarchical DBSCAN (HDBSCAN) algorithm was applied to the woody point cloud to segment individual branch clusters[28]. For each branch, a straight line was fitted using the Random Sample Consensus (RANSAC) algorithm[29], and the angle between the line

Table 1. Overview of the ground-based survey of representative phenotypic traits used in the traditional *P. chinensis* clonal selection.

Traits (unit)	Range	Mean ± standard deviation
Plant height (m)	0.48–1.65	1.14 ± 0.26
Scion diameter (mm)	7.48–30.36	20.05 ± 5.62
Crown width (m)	0.19–1.11	0.62 ± 0.21
Mean angle of first-order branches (°)	16.50–67.83	37.59 ± 11.79
Number of compound leaves (pieces)	6–85	29 ± 14

and the vertical axis was calculated. The branch exhibiting the smallest deviation from vertical was identified as the main stem, while all others were designated as first-order branches. Subsequently, branch angles relative to the main stem were computed (Eq. [2]). Following wood segmentation, compound leaves were extracted from the remaining leaf point cloud using DBSCAN clustering. Representative examples of leaf–wood separation and branch determination are shown in Fig. 3.

$$\theta = arccos\left(\frac{\vec{d_1}\cdot\vec{d_2}}{\left\|\vec{d_1}\right\|\left\|\vec{d_2}\right\|}\right), \quad (2)$$

here $\vec{d_1}$ and $\vec{d_2}$ are the directional vectors of the first-order branch and the main stem.

UAV data and preprocessing

The UAV multispectral and RGB imagery were acquired under clear sky conditions on November 12, 2024. A DJI Mavic 3 Multispectral UAV system was employed. The flight parameters were set as follows: 75% side overlap and 80% forward overlap; flight altitude of 25 m; ground sampling distance (GSD) of 1.18 cm for multispectral images and 0.69 cm for RGB images, and flight speed of 1.6 m/s. Three reflectance reference panels with reflectance of (25%, 50% and 75%) were placed on the ground near the nursery for reflectance correction of multispectral images. The UAV-based multispectral and RGB orthomosaics were generated using MetaShape, which requires the following steps: image alignment, dense point cloud generation, digital surface model (DSM) generation, and orthomosaic generation. The reflectance correction of the multispectral orthomosaic was performed using an empirical line model based on the three reference panels[30].

Extraction of structure-related traits

To comprehensively characterize the multi-branched habit and complex canopy architecture of *P. chinensis* seedlings, we extracted a suite of structural traits from multiple dimensions, encompassing growth traits, morphological traits, and architectural complexity. A total of 14 structural traits were derived from the TLS point cloud of each seedling (Table 2). Plant height was calculated as the difference between the maximum and minimum Z-axis (i.e., vertical) coordinates of each seedling's point cloud. To quantify crown width, the point cloud was first projected onto the horizontal (XY) plane, and the average of crown extents in the X (East-West) and Y (North-South) directions was then computed. To determine the maximum crown height, we stratified the entire crown into horizontal layers at 0.1 m vertical intervals, and identified the height at which the maximum stratified crown width occurred. The projection area was calculated by projecting the point cloud onto the horizontal (XY) plane and overlaying a 1-cm-resolution grid. The total area was determined as the number of occupied grids multiplied by the area of a single grid. Convex hull area was derived by projecting the point cloud onto the horizontal (XY) plane and computing the area of the minimum bounding convex polygon using Delaunay triangulation. Projection compactness was obtained by dividing the ratio of projection area by the convex hull area. Voxel-based volume was estimated by partitioning the 3D space into 2 cm-resolution voxels and counting the number of voxels occupied by points, then calculated as the product of occupied voxel count and single voxel volume, and converted to cubic centimeters. Convex hull volume was calculated by constructing the minimum bounding convex polyhedron that fully enclosed the 3D point cloud, using the Qhull

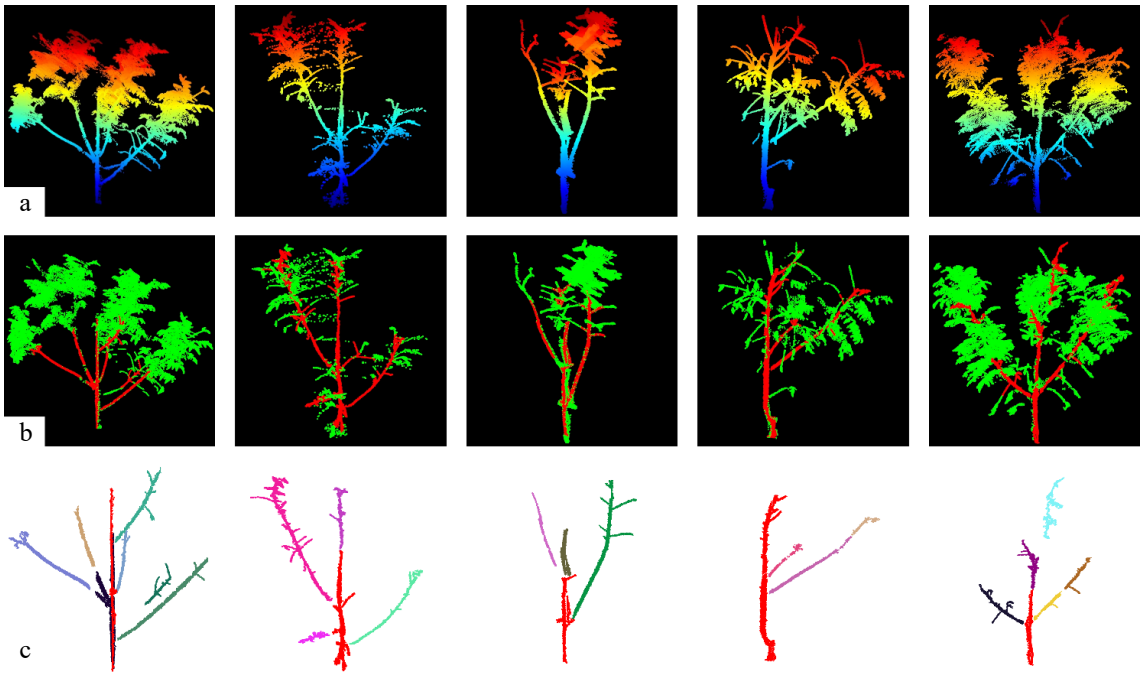

Fig. 3 (a) Visualization of representative *Pistacia chinensis* seedling point clouds, (b) separation of leaf and woody components, and (c) segmentation of the main stem and first-order branches, where different colors indicate different first-order branches.

Table 2. Summary of TLS-derived structural traits of *Pistacia chinensis* seedlings.

Types	Traits (abbreviation)	Definition	Ref.
Growth traits	Plant height (PH)	Height of an individual seedling	[31]
	Crown width (CW)	Mean crown width in the X and Y directions	[31]
	Crown width ratio (CWR)	Ratio of crown width to plant height	[31]
	Maximum crown height (MCH)	The height corresponding to the layer with the largest crown width was recorded	[31]
Morphological traits	Projection area (PA)	Vertically projected area of the crown of an individual seedling	[18]
	Convex-hull area (CA)	Convex hull area of an individual seedling in the XY plane for the vertically-projected point cloud	[18]
	Voxel-based volume (VV)	Volume of the voxelized crown of an individual seedling	[18]
	Convex-hull volume (CV)	Volume of the convex hull of the crown of an individual seedling	[18]
	Projection compactness (PC)	Ratio of projection area to convex-hull area	[18]
	Volume compactness (VC)	Ratio of voxel-based volume to convex-hull volume	[18]
	Canopy occupation volume (COV)	Ratio of the number of occupied voxels to the total number of voxels	[32]
	Mean of first-order branch angles (MFBA)	Mean of the angles between first-order branches and the main stem.	[33]
	Relative leaf abundance	Ratio of the number of compound leaves at a specific layer to the total number of those in all layers (LCLP, MCLP UCLP)	[33]
Architecture complexity	Canopy entropy (CE)	A metric to simplify forest canopy structural complexity and spatial heterogeneity.	[19]

algorithm. Volume compactness was obtained by dividing the ratio of voxel-based volume by convex hull volume. The canopy occupation volume was obtained by first generating a bounding box around the outermost points of the canopy point cloud, which was then divided into voxels of 0.02 m in size. Voxels containing any point cloud data were considered occupied, and the canopy occupation volume was calculated as the ratio of occupied voxels to the total number of voxels within the bounding box. The mean of first-order branch angles was already described in TLS data and preprocessing. Relative compound leaf abundance was used to characterize the vertical distribution of compound leaves within the canopy. To calculate this trait, plant height was divided into three vertical segments: lower (10%–40% of total height), middle (40%–70%), and upper (70%–100%). The number of compound leaves within each segment was counted, and their proportions relative to the total number of compound leaves were computed. These were defined as the lower-layer compound leaf proportion (LCLP), middle-layer compound leaf proportion (MCLP), and upper-layer compound leaf proportion (UCLP), respectively. The calculation of canopy entropy began with projecting the 3D point cloud of each seedling onto the three orthogonal 2D planes (XY, XZ, and YZ). Kernel density estimation (KDE) was then applied to each projection to derive the spatial probability density function. Based on the estimated densities, directional entropy values were computed using Monte Carlo integration[19]. These values were finally averaged to obtain a composite canopy entropy index, providing an integrated measure of canopy spatial heterogeneity and structural complexity.

To investigate the dimensional structure of the phenotypic dataset, Spearman's correlation analysis was performed among the structural and spectral traits to identify potential interactions and dependencies between phenotypic dimensions.

Extraction of spectra-related traits

To accurately characterize the spectral characteristics of *P. chinensis* clonal seedlings, we employed eight vegetation indices that have been reported to be sensitive to leaf pigment content and plant physiological status (Table 3)[34]. For each seedling, the canopy boundary was delineated through visual interpretation and manually digitized as an irregular, edge-following polygon mask. Non-vegetation pixels inside the mask were then removed using the Optimized Soil-Adjusted Vegetation index (OSAVI), and a fixed threshold of 0.3, based on UAV-based multispectral imagery. The refined canopy mask was applied to both multispectral and RGB images for vegetation index calculation. Owing to the absence of a blue band in the UAV-based multispectral sensor, indices requiring the blue band were computed using the corresponding RGB imagery. To minimize ambient light effects, relative radiometric normalization was performed using standard reflectance panels imaged before, and after each flight, with fixed exposure and white balance settings. To reduce the influence of residual mixed pixels and local radiometric anomalies, a Z-score method was used for each vegetation index, whereby pixels with values exceeding three standard deviations from the seedling mean were excluded from further analysis.

Comprehensive provenance evaluation and clonal selection

To evaluate phenotypic differences among seedlings from different provenances, we conducted a comprehensive provenance evaluation. Principal Component Analysis (PCA) was applied to the standardized structural and spectral trait datasets to reduce dimensionality. Based on the PCA results, an overall composite score (F_total) was calculated for each seedling as the weighted sum of its

Table 3. Summary of vegetation indices calculated based on multispectral or RGB imagery.

Sensor	Vegetation indices	Formula	Ref.
Multispectral	Normalized Difference Vegetation Index (NDVI)	$NDVI = \frac{NIR_m - R_m}{NIR_m + R_m}$	[34]
	Normalized Difference Red Edge Index (NDRE)	$NDRE = \frac{NIR_m - RE_m}{NIR_m + RE_m}$	[35]
	Chlorophyll Leaf Senescence Index (CLSI)	$\mathrm{CLSI} = \frac{RE_m - G_m}{RE_m + G_m} - RE_m$	[36]
	Weighted Difference Vegetation Index (WDRVI)	$\mathrm{WDRVI} = \frac{\alpha \cdot NIR_m - R_m}{\alpha \cdot NIR_m + R_m}$	[37]
RGB	Excess Green Index (EXG)	$\mathrm{EXG} = 2 \times G_v - R_v - B_v$	[34]
	Normalized Green-Red Difference Index (NGRDI)	$\mathrm{NGRDI} = \frac{G_v - R_v}{G_v + R_v}$	[38]
	Red-Green Ratio Index (RGRI)	$\mathrm{RGRI} = \frac{R_v}{G_v}$	[39]
	Red Chromatic Coordinate (RCC)	$\mathrm{RCC} = \frac{R_v}{R_v + G_v + B_v}$	[34]

Note that the indices requiring the blue band were computed using the corresponding RGB imagery. The subscripts m and v denote multispectral and visible (i.e., RGB), respectively.

principal component scores, where weights were determined by the variance contribution ratio. One-Way Analysis of Variance (ANOVA) followed by Tukey's Honestly Significant Difference (HSD) post hoc tests were conducted on the composite scores to assess phenotypic differences among provenances[40]. Additionally, Pearson correlation analysis was performed to evaluate the relationships between structural and spectral traits, and to assess the redundancy or complementarity of the multi-modal data. Correlation coefficients (r) were visualized using a heatmap. This comprehensive analysis enabled the identification of key traits contributing to provenance differentiation and provided a robust basis for elite clonal selection. Furthermore, to partition seedlings into a small number of interpretable phenotypic 'types' for subsequent trait summarization and application-oriented selection, K-means clustering was applied to the PCA-reduced feature space, where principal components are orthogonal and comparable in scale, making Euclidean-distance–based compact clustering appropriate and providing clear cluster centroids as phenotype prototypes. The optimal number of clusters was determined using the elbow method. These phenotypic clusters were then evaluated in the context of application-specific requirements, allowing for the targeted recommendation of potential cultivars based on their structural and spectral traits.

Results

Validation of structure-related traits derived by TLS

Figure 4 shows the comparison of four commonly used structural traits between TLS-derived and manual measurements, to evaluate the effectiveness and accuracy of TLS-based measurements. The comparative analysis revealed significant linear relationships between the TLS-derived phenotypic traits and manual measurement. TLS exhibited the highest accuracy in estimating plant height (R^2 = 0.91; rRMSE = 6.58%). In contrast, its performance in quantifying the number of compound leaves was comparatively lower (R^2 = 0.71; rRMSE = 12.45%). For 2D traits such as plant height and crown width, TLS-derived values were generally reliable, although a few extreme values were observed at the distribution boundaries. Regarding 3D traits including the number of compound leaves and the mean of first-order branch angles, TLS-derived also demonstrated robust performance. Specifically, when the number of compound leaves ranged between 20 and 40, the data points were tightly clustered around the regression line. However, accuracy tended to decline as leaf number increased, with TLS-derived values consistently underestimating values compared to manual measurement. For the mean of first-order branch angles, although accuracy was slightly less stable than that of 2D traits, deviations remained within acceptable limits, supporting the feasibility of using TLS-derived data for downstream structural trait extraction.

Correlation among structural and spectral traits

Table 4 summarizes descriptive statistics (mean, standard deviation, minimum, maximum, and coefficient of variation, CV) for all 14 TLS-derived structural traits (Table 2) and the 8 UAV-derived spectral traits (Table 3) across the entire seedling population. The results indicate substantial between-individual variability for many traits, revealing pronounced phenotypic heterogeneity within the population. This level of variation supports the need for subsequent correlation analysis, PCA, and trait-based clustering to characterize and classify distinct phenotypic types.

Based on Spearman's correlation analysis (Fig. 5), most structural and spectral traits exhibited no significant linear relationships, confirming that they describe phenotypic traits from distinct and complementary dimensions. Notably, greenness indices (EXG, NDVI) exhibited strong positive correlations with volume and compactness traits (VV, PC, VC), but negative correlations with canopy complexity (UCLP, CE). Regarding structure, the MFBA was positively correlated with 2D morphological traits, but negatively with compactness (PC, VC, COV), indicating that taller seedlings with spreading branches tend to exhibit lower canopy density. Furthermore, structural complexity metrics (CE, UCLP) showed significant negative correlations with compactness, implying that complex branching patterns lead to more irregular canopies. Among vegetation indices, visible-light metrics (EXG, NGRDI) were strongly correlated with NDVI, while multispectral indices (e.g., CLSI) captured independent variations, collectively enhancing the robustness of phenotypic assessments. To facilitate visual assessment of relationship patterns (e.g., linearity and potential outliers), scatter plots for representative trait pairs (or a scatter-plot matrix) are provided in Supplementary Fig. S1.

Evaluation of phenotypic differences among provenances

Figure 6 shows the feature loadings of structural and spectral traits derived from PCA. The first three principal components (PC1, PC2, and PC3) collectively accounted for 63.09% of the total variance, with PC1 explaining 34.48%, PC2 accounting for 18.29%, and PC3 contributing 10.32%. PC1 was strongly associated with structural traits such as voxel-based volume (VV), convex hull volume (CV), convex hull area (CA), plant height (PH), and crown width (CW), all of which exhibited high positive loadings. These results indicate that PC1 primarily captures variation in overall seedling structural scale and spatial extent. PC2 was mainly related to a combination of morphological and spectral traits, including projection compactness (PC), volume compactness (VC), proportion of upper compound leaves (UCLP), the normalized difference vegetation index (NDVI), and the weighted difference vegetation index (WDRVI). This suggests that PC2 represents an integrated dimension combining structural morphology and leaf pigmentation characteristics. In contrast, PC3 was dominated by vegetation indices such as the red-green ratio index (RGRI), red chromatic coordinate (RCC), and canopy leaf structure index (CLSI), highlighting its focus on describing seedling variation from a leaf coloration perspective. Taken together, these findings demonstrate that phenotypic divergence among *P. chinensis* clonal populations is primarily driven by growth traits, morphological traits, and the interplay between structural and spectral traits.

Figure 7 shows the polar plot of the F-total value for each clone population. Based on a weighted linear combination of the first 11 principal components (with a cumulative variance contribution of 95.41%), this study calculated a comprehensive score (F-total) for each *Pistacia chinensis* clonal seedling to evaluate its overall performance across structural and spectral trait dimensions. The results showed that F-total varied significantly among provenances and clones, ranging from −1.26 to 1.57, indicating that the score effectively captured the dispersion of clones in terms of integrated phenotypic traits. Moreover, F-total demonstrated good discriminative power among clonal lines, providing a quantitative basis for elite clone selection.

Figure 8 illustrates that provenance had a significant effect on this trait, as indicated by ANOVA (F = 5.013, p < 0.001), demonstrating substantial variation among provenances. Post hoc comparisons

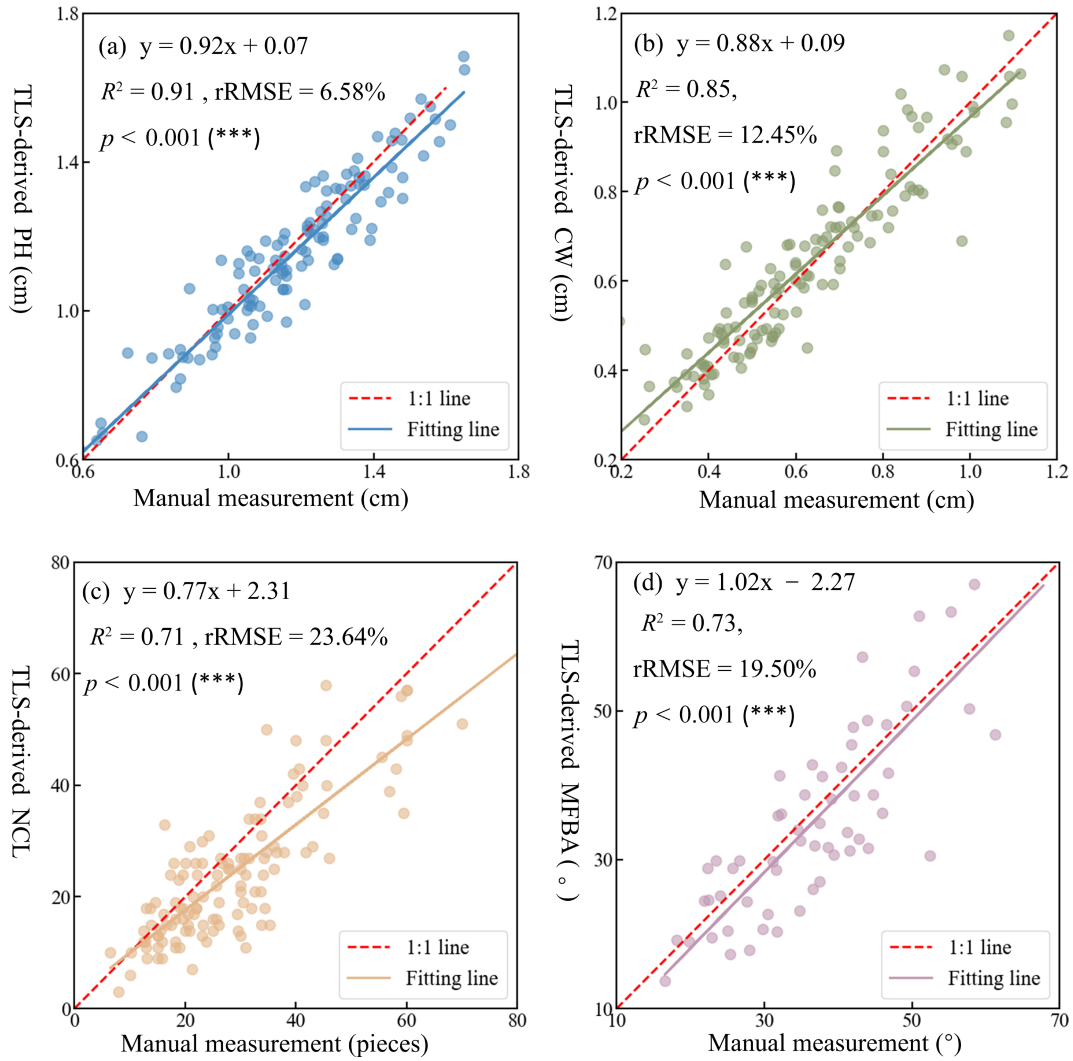

Fig. 4 Comparison between TLS-derived and manually-measured structural traits of *Pistacia chinensis* seedlings. (a) Plant height, (b) crown width, (c) number of compound leaves, and (d) mean of first-order branch angles.

using the Tukey HSD test identified several significant pairwise differences ($p < 0.05$). In particular, provenance WJC differed significantly from H2 ($p < 0.001$), J2 ($p = 0.0090$), LGC ($p = 0.0234$), YJA ($p = 0.0004$), and YX ($p = 0.0267$). Additionally, H2 showed significant differences when compared with LGC ($p = 0.0016$) and MAS ($p = 0.0132$). These results indicate that WJC exhibited the most pronounced divergence in this trait relative to other provenances. A heatmap summarizing the significance of pairwise differences (Fig. 8) provides a visual overview of these patterns.

Clonal selection based on K-means

Following PCA dimensionality reduction, unsupervised k-means clustering was performed, and the elbow method identified four as the optimal number of clusters. As shown in Figs 9 and 10, the *P. chinensis* clonal seedling population was thus classified into four distinct groups, each exhibiting unique trait differences and characteristics. Type 1 seedlings are characterized by compound leaves concentrated in the upper canopy, accompanied by relatively low area and volume. Both PC and VC are comparatively low, indicating a loosely arranged spatial structure. However, these seedlings display lower EXG and NDVI values but higher NDRE and CLSI indices. This pattern suggests that seedlings in this type are likely at the post-color change stage, with reddening leaves, expanded branches and foliage, and relatively tall branch bases. Type 2 seedlings exhibit reduced plant height and crown width, as well as low volume and area. Despite this, PC, VC, and COV reach their highest values, while MFBA is minimal, and CE is maximal. Regarding leaf color indices, this group shows elevated NDVI, NDRE, and WDRVI values, with other vegetation indices spanning broadly. Notably, this type has the lowest total PCA score (F-total). These traits indicate that these seedlings are in the color change phase, characterized by short stature, high compactness, and slower growth. Type 3 seedlings are marked by greater plant height and crown width, as well as higher volume and area. They possess high MFBA, but low CE values. EXG and NDVI indices are elevated, whereas RCC, CLSI, and NDRE are relatively low. This type also attains the highest F-total scores, indicative of vigorous growth, abundant and well-developed branches, and an orderly branching structure without entering the color change stage. Type 4 seedlings represent a uniform group, with most traits around average values, thereby classified as an intermediate type. This type of approach provides a robust framework for classifying *P. chinensis* seedlings during the nursery stage, enabling early selection of superior individuals and enhancing subsequent breeding efficiency.

Table 4. Descriptive statistics of TLS-derived structural traits and UAV-derived spectral traits across the entire seedling population.

Traits	Mean	SD	Min	Max	CV %
PH	1.11	0.25	0.55	1.69	22.71
CW	0.64	0.21	0.29	1.15	32.78
CWR	0.58	0.15	0.33	1.01	25.06
PA	0.19	0.12	0.05	0.54	60.48
CA	0.30	0.19	0.06	0.97	64.21
VV	29,265.82	20,693.74	5,224.00	100,144.00	70.71
CV	185,124.08	144,665.50	20,731.35	580,001.78	78.15
PC	0.67	0.13	0.27	0.92	19.01
VC	0.18	0.08	0.05	0.45	40.80
COV	0.33	0.12	0.15	0.73	35.44
MFBA	18.22	20.51	0.00	77.09	112.61
LCLP	0.53	0.19	0.24	1.00	35.85
MCLP	0.33	0.14	0.00	0.67	42.05
UCLP	0.14	0.11	0.00	0.44	80.25
CE	1.40	0.94	0.47	3.93	67.12
EXG	0.21	0.17	−0.23	0.55	80.93
NGRDI	−0.39	0.24	−1.19	0.01	62.64
RGRI	1.36	0.51	−0.59	2.56	37.65
RCC	0.41	0.26	−0.34	1.07	63.36
NDVI	0.41	0.14	−0.03	0.66	34.14
NDRE	0.03	0.04	−0.06	0.14	117.42
CLSI	−0.03	0.08	−0.24	0.19	238.25
WDRVI	−0.71	0.04	−0.85	−0.64	6.12

Note: CV (%) = SD/mean × 100%.

Discussion

Multi-modal proximal sensing enhances phenotypic analysis for colored-leaf seedlings

Our results demonstrate that the integration of TLS and UAV-based imagery facilitates synergistic observation and comprehensive extraction of both structural and spectral traits in colored-leaf seedlings. TLS primarily captures 2D and 3D structural traits. The agreement between TLS-derived and manually measured values for four commonly used structural traits highlights the potential of TLS to reliably characterize the structural traits of small-size seedlings. Notably, relatively large errors observed in the estimation of compound leaf number and mean angle of first-order branches were likely attributable to the small size of these structures near the seedling apex, where their dimensions approach the ranging resolution limits of TLS. The present study did not include validation of spectral traits, as numerous previous studies have demonstrated the effectiveness of vegetation indices in characterizing leaf pigmentation and color variation[34, 41]. This pattern is consistent with previous findings and underscores the need for integrating multi-modal data to enable comprehensive trait quantification[42,43]. In this study, NDVI showed moderate positive correlations with VV (r = 0.41), PC (r = 0.43), and VC (r = 0.40). These associations may reflect that seedlings with larger crowns have higher leaf area index, contributing to increased NDVI values. Additionally, variation in PC and VC likely influences light interception efficiency, thereby affecting internal chlorophyll content.

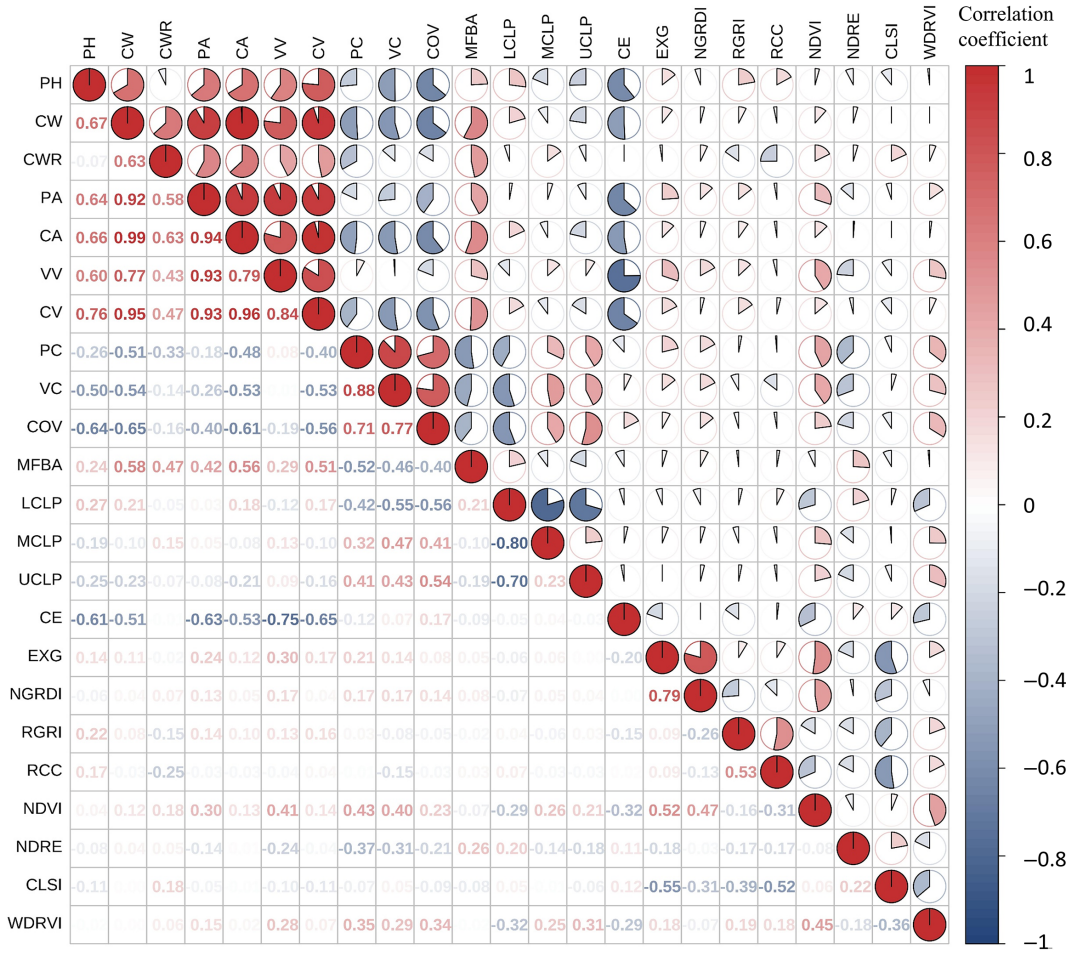

Fig. 5 Spearman's correlation analysis for structural and spectral traits of *Pistacia chinensis* seedlings.

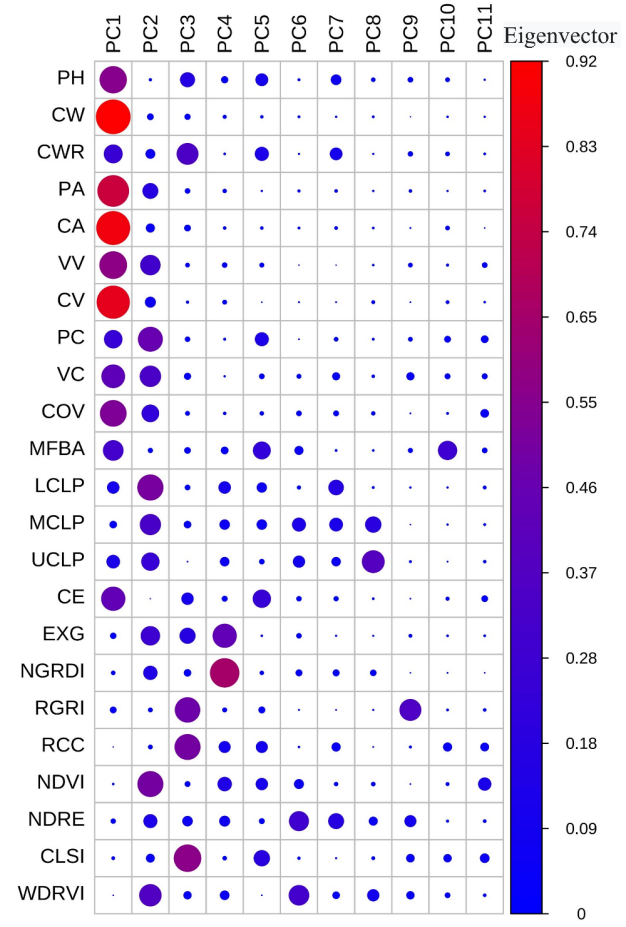

Fig. 6 Normalization of the structural and spectral traits of all seedlings using PCA.

Our PCA results indicate that PC1 is predominantly influenced by morphological and growth traits. Instead, PC2 and PC3, which reflect tree architecture and leaf coloration, are more relevant for cultivar selection in ornamental species. These traits are challenging to measure in the field but can be efficiently captured via near-ground remote sensing. Our analysis indicates that relying on any single structural or spectral trait is inadequate for comprehensively characterizing the phenotypic differentiation among *P. chinensis* seedlings. The weak correlation observed between structural and spectral traits (Fig. 5) suggests that they capture distinct and complementary phenotypic dimensions; relying solely on one overlooks the other. Furthermore, the PCA results (Fig. 6) revealed that the phenotypic variation is driven by a composite of factors: physiological scale (dominated by PC1), structure-color coupling (PC2), and specific foliage coloration (PC3). This implies that the divergence among provenances stems from the interplay of multidimensional traits rather than a single attribute. Our comprehensive evaluation confirmed significant provenance-level differences, validating that this multi-modal phenotyping pipeline can rapidly and effectively identify germplasm resources. While some provenances showed subtle distinctions, the Tukey HSD post hoc test successfully identified statistically discrete groups, which is crucial for the selection and breeding of new cultivars.

Elite clone selection of colored-leaf seedlings benefits from structural and spectral traits

This study conducted elite clone selection using the K-means method based on structural and spectral traits of seedlings. Due to

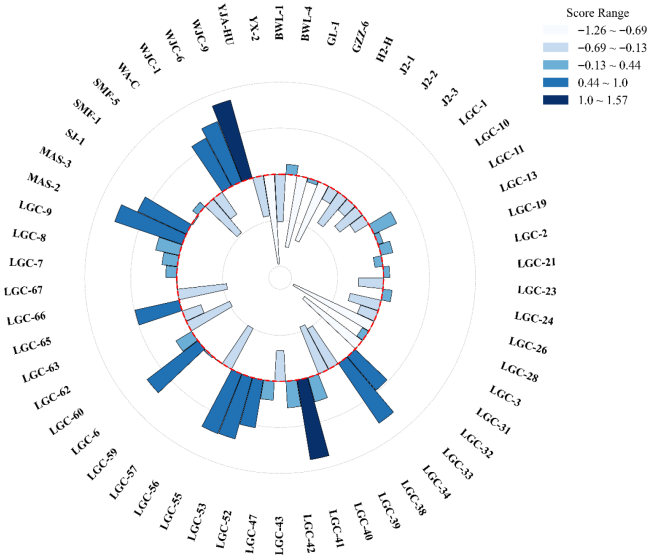

Fig. 7 The F-total value of each *Pistacia chinensis* clone seedling, indicating the phenotyping differences. The alphabetical prefix (e.g., 'LGC) represents the provenance origin, and the numerical suffix (e.g., '28') identifies the specific clonal lineage within that provenance.

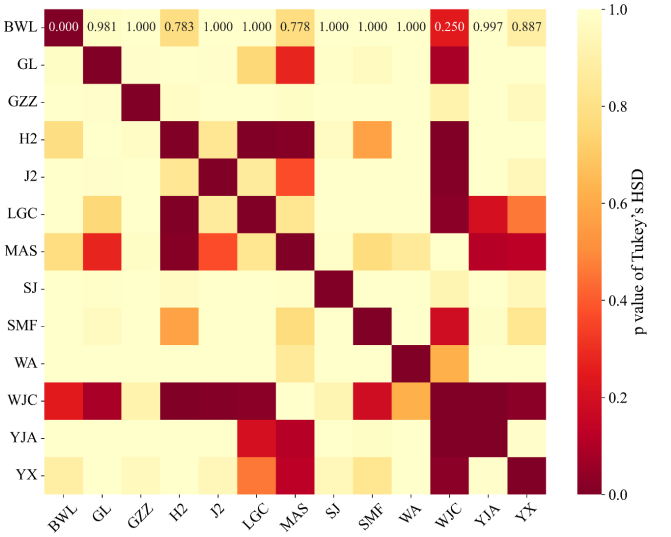

Fig. 8 Heatmap showing the results of pairwise Tukey's HSD tests for differences in F-total among provenances. The color gradient reflects the level of significance, with darker shades indicating lower *p*-values. Provenances such as WJC and H2 exhibited significant divergence from several others, underscoring provenance-level variation in this trait.

the unsupervised nature of K-means clustering[44], it effectively groups seedlings with similar structural and spectral characteristics. As shown in Fig. 9, each cluster displays distinct phenotypic profiles that differ significantly from those of other groups. While a weak dependency was observed between spectral and structural traits, the correlation was not strong.

For instance, in type 1, most seedlings with this structural phenotype exhibited signs of foliar coloration, yet the specific hues and degrees of color change varied widely, suggesting limited consistency. In contrast, type 3 seedlings showed a more spreading branching pattern and vigorous growth, with leaves mostly remaining light green, possibly due to the delayed onset of senescence. Types 2 and 4, however, showed no obvious correspondence between structure and spectral features. These clustering results offer a practical framework for early-stage phenotypic screening

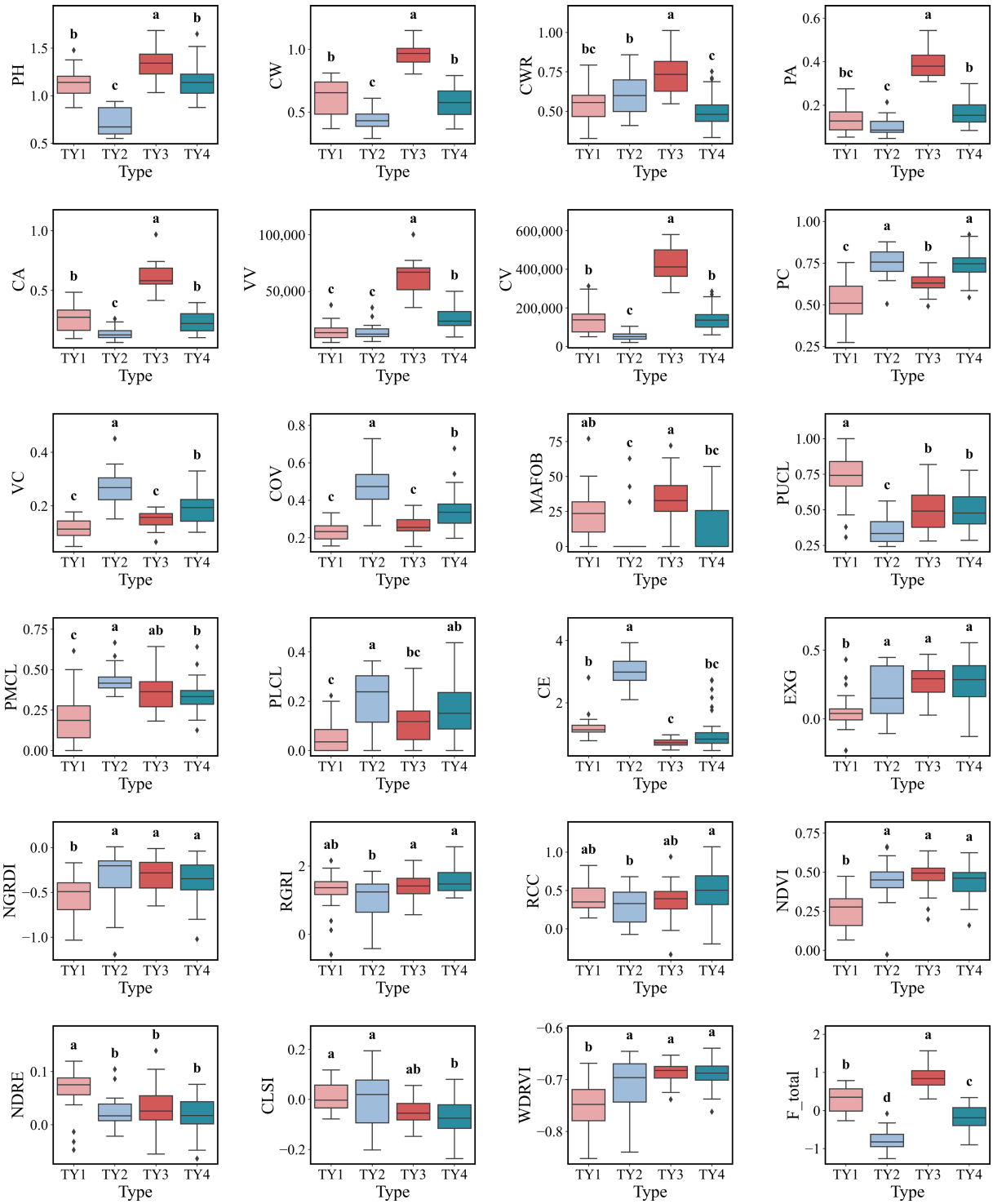

Fig. 9 Box plots of phenotypic traits for the four clusters identified by K-means clustering. The horizontal line within the box indicates the median, boundaries of the box indicate the 25th and 75th percentiles, and whiskers indicate the range. Different lowercase letters (a, b, c, d) above the boxes indicate statistically significant differences among the four clusters based on One-way ANOVA followed by Tukey's HSD test ($p < 0.05$).

tailored to future landscape applications. For example, type 1 seedlings, characterized by straight stems, high clear boles, and extended coloration periods, may be ideal for street tree planting. Type 3, with its prominent spreading and orderly branching, is potentially well-suited for ornamental landscaping. Meanwhile, type 2 seedlings, being compact and relatively short, may be more resilient and suitable for harsh site conditions.

It is important to note that PCA-based ranking inherently maximizes statistical variance interpretation rather than directly defining 'optimal' breeding value. Therefore, the F-total provided in this study serves as a baseline for phenotypic diversity. For practical breeding applications: Landscaping scenarios, breeders should prioritize traits associated with aesthetic value. In this context, higher weights should be assigned to spectral traits (e.g., leaf color durability, redness) and crown shape metrics (e.g., compaction), utilizing the clusters characterized by vibrant foliage (e.g., type 2). For afforestation/timber scenarios, the focus should shift to growth potential and biomass accumulation. Structural traits such as plant

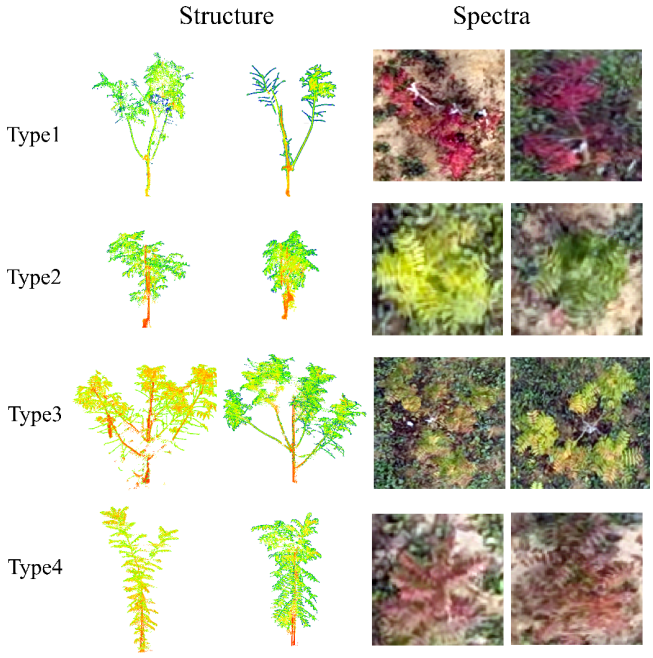

Fig. 10 Two representative individuals were selected from distinct clonal types of *P. chinensis* to illustrate structural (point cloud) and spectral (RGB imagery from UAV) characteristics, highlighting marked phenotypic differences between types.

height, crown volume, and branch angles should be the primary selection criteria, favoring vigorous growth types (e.g., type 1).

Limitations and potential solutions

Although this study presents an effective approach for identifying a broad range of structural and spectral traits in colored-leaf seedlings using multi-modal proximal sensing and supports elite clonal selection tailored to target applications, several limitations and uncertainties remain regarding the experimental implementation and phenotypic characterization. First, multi-modal proximal sensing observations and field surveys were conducted at a single time point, limiting the ability to capture temporal dynamics and trait responses throughout the growing season. Both structural and spectral traits are known to exhibit seasonal variation, which may influence the accuracy and generality of phenotypic assessments. Moreover, the timing, onset, and duration of leaf coloration were not considered in this study, potentially overlooking important phenological cues relevant to clonal selection. To address these issues, future research will involve collecting long-term time-series data of *P. chinensis* clonal seedlings spanning from May to November, encompassing both the growing season, and the leaf coloration phase. Observations should be conducted monthly during the growing season and biweekly during the coloration period to fully characterize the temporal dynamics of structural and spectral traits. In particular, for the key trait of leaf coloration, multitemporal UAV imagery combined with phenological information will be used to determine the timing and progression of color change.

Second, the extraction of complex structural traits, such as branch angles and the number of compound leaves, still suffers from limited automation, with most algorithms requiring manual parameter tuning. Future work should focus on the development of improved adaptive algorithms to enhance automation and robustness. Furthermore, to enable efficient processing of multimodel datasets, automatic seedling detection and segmentation remain a critical bottleneck. In this context, deep learning approaches hold promise for achieving high-throughput, automated identification and extraction of seedling regions across large-scale datasets.

Third, while feature-level integration avoids complex registration errors, the lack of 3D spectral information limits the assessment of lower-canopy leaves. Future research could employ 3D reconstruction techniques (e.g., photogrammetry or LiDAR-camera fusion) to map spectral information onto 3D point clouds. This would enable voxel-based spectral analysis, allowing for the precise separation of leaves and background at different canopy layers, thereby optimizing the accuracy of whole-plant phenotyping.

Fourth, the juvenile-mature correlation is a fundamental consideration in woody plant breeding[45]. We acknowledge that predicting adult performance solely from seedling phenotypes involves uncertainty, as trait expression can be influenced by ontogenetic changes and environmental interactions over time. However, delaying selection until maturity is often impractical due to the long generation intervals of tree species. According to forest genetics theory, early selection based on seedling traits is a vital strategy to maximize genetic gain per unit time[46]. Although the genetic correlation between early and late traits typically increases with age, selecting for early structural vigor (e.g., height, crown volume) and physiological potential (e.g., pigment content) effectively filters out inferior germplasm. This process significantly shortens the breeding cycle and enhances breeding efficiency by focusing resources on a smaller, elite population for long-term testing.

Conclusions

This study demonstrates the efficacy of integrating TLS and UAV-based multispectral/RGB imaging as a practical approach for phenotyping and early selection of Pistacia chinensis clonal seedlings. By synergistically capturing 3D structural traits (e.g., projection compactness, volume compactness, mean of first-order branch angles) and spectral traits (e.g., NDVI, EXG, CLSI), we established a multi-modal proximal sensing framework that effectively addresses the limitations of manual surveys and single-source remote sensing. Key findings include (1)Significant phenotypic differences were observed among Pistacia chinensis clonal seedlings, and these differences could be effectively characterized through the synergistic analysis of structural and spectral traits. (2)Distinct phenotypic variations were also identified among different provenances of Pistacia chinensis clonal seedlings, providing important insights into provenance-level phenotypic variation patterns. (3)Based on the K-means clustering results, the Pistacia chinensis clonal seedling population in the study area could be classified into four phenotypic types, providing a scientific basis for elite clone selection and classification. In conclusion, this pipeline provides a reliable multi-source remote sensing solution for the early selection of color-leaved tree species by linking early seedling phenotypes to functional traits.

Author contributions

The authors confirm their contributions to the paper as follows: writing – original draft, visualization, software, methodology, investigation: Zhang D; methodology, funding acquisition, conceptualization: Chen L; writing – review and editing, supervision, methodology, funding acquisition, conceptualization: Li L; visualization, methodology: Bai Q; visualization, software, methodology: Yu Z; resources, data curation: Jiang X, Liu J; funding acquisition, supervision, conceptualization: Huang H. All authors reviewed the results and approved the final version of the manuscript.

Data availability

The datasets generated during and/or analyzed in the current study are available from the corresponding author on reasonable request.

Acknowledgments

This work was supported by the Fundamental Research Funds for the Central Universities (Grant No. QNTD202510) and the Open Fund of State Key Laboratory of Remote Sensing Science (Grant No. OFSLRSS202423). We thank Dr. Qingsong Yang from Beijing Forestry University for providing theoretical support for the helpful discussion on selection of color-leaved tree seedlings.

Conflict of interest

The authors declare that they have no conflict of interest.

Supplementary information accompanies this paper online at: https://doi.org/10.48130/smartfor-0026-0005.

Dates

Received 24 December 2025; Revised 26 February 2026; Accepted 17 March 2026; Published online 26 May 2026

References

[1] Yang C, Li MY, Li T, Ren F, Li DP, et al. 2023. Scenic beauty evaluation of forests with autumn-colored leaves from aerial and ground perspectives: a case study in Qixia mountain in Nanjing, China. *Forests* 14:542

[2] Bai Q, Su S, Lin Z, Leng P, Wang W. 2016. The variation characteristics and blooming phenophase of monoecious *Pistacia chinensis* Bunge. *HortScience* 51:961–967

[3] Guo Y, Zhao Z, Zhu F, Gao B. 2023. The impact of global warming on the potential suitable planting area of *Pistacia chinensis* is limited. *Science of the Total Environment* 864:161007

[4] Li HL, Zhang ZX, Lin SZ, Li XX. 2007. Research advances in the study of *Pistacia chinensis* Bunge, a superior tree species for biomass energy. *Forestry Studies in China* 9:164–168

[5] Kim SL, Chung YS, Silva RR, Ji H, Lee H, et al. 2019. The opening of phenome-assisted selection era in the early seedling stage. *Scientific Reports* 9:9948

[6] Krings A. 2011. Pistacia chinensis (Anacardiaceae) naturalized in north Carolina, USA. *Journal of the Botanical Research Institute of Texas* 5(2):867–869

[7] Fan J, Zhang Y, Wen W, Gu S, Lu X, et al. 2021. The future of internet of things in agriculture: plant high-throughput phenotypic platform. *Journal of Cleaner Production* 280:123651

[8] Zhang M, Xu S, Han Y, Li D, Yang S, et al. 2023. High-throughput horticultural phenomics: the history, recent advances and new prospects. *Computers and Electronics in Agriculture* 213:108265

[9] Fan L, Yang J, Wang X, Liu Z, Xu B, et al. 2025. Combining UAV multi-sensor field phenotyping and genome-wide association studies to reveal the genetic basis of plant height in cotton (*Gossypium hirsutum*). *Plant Phenomics* 7:100026

[10] Jin S, Su Y, Zhang Y, Song S, Li Q, et al. 2021. Exploring seasonal and circadian rhythms in structural traits of field maize from LiDAR time series. *Plant Phenomics* 2021:9895241

[11] Li L, Liu S, Wang Z, Zhao X, Qi J, et al. 2025. Seeing into individual trees: tree-specific retrieval of tree-level traits using 3D radiative transfer model and spatial adjacency constraint from UAV multispectral imagery. *Remote Sensing of Environment* 318:114616

[12] Li L, Huang H, Mu X, Yan G, Qi J, et al. 2025. Low-altitude UAV-based quantitative remote sensing of vegetation: advances, challenges, and prospects. *National Remote Sensing Bulletin* 29(6):2083–2113

[13] Xie C, Yang C. 2020. A review on plant high-throughput phenotyping traits using UAV-based sensors. *Computers and Electronics in Agriculture* 178:105731

[14] Zhao X, Qi J, Yu Z, Yuan L, Huang H. 2024. Fine-scale quantification of absorbed photosynthetically active radiation (APAR) in plantation forests with 3D radiative transfer modeling and LiDAR data. *Plant Phenomics* 6:0166

[15] Jin S, Su Y, Wu F, Pang S, Gao S, et al. 2019. Stem–leaf segmentation and phenotypic trait extraction of individual maize using terrestrial LiDAR data. *IEEE Transactions on Geoscience and Remote Sensing* 57:1336–1346

[16] Zhu Y, Sun G, Ding G, Zhou J, Wen M, et al. 2021. Large-scale field phenotyping using backpack LiDAR and CropQuant-3D to measure structural variation in wheat. *Plant Physiology* 187:716–738

[17] Gao W, Yang X, Cao L, Cao F, Liu H, et al. 2023. Screening of ginkgo individuals with superior growth structural characteristics in different genetic groups using terrestrial laser scanning (TLS) data. *Plant Phenomics* 5:0092

[18] Chen H, Zhang M, Xiao S, Wang Q, Cai Z, et al. 2024. Quantitative analysis and planting optimization of multi-genotype sugar beet plant types based on 3D plant architecture. *Computers and Electronics in Agriculture* 225:109231

[19] Liu X, Ma Q, Wu X, Hu T, Liu Z, et al. 2022. A novel entropy-based method to quantify forest canopy structural complexity from multiplatform lidar point clouds. *Remote Sensing of Environment* 282:113280

[20] Bhandari M, Ibrahim AMH, Xue Q, Jung J, Chang A, et al. 2020. Assessing winter wheat foliage disease severity using aerial imagery acquired from small Unmanned Aerial Vehicle (UAV). *Computers and Electronics in Agriculture* 176:105665

[21] Kerkech M, Hafiane A, Canals R. 2018. Deep leaning approach with colorimetric spaces and vegetation indices for vine diseases detection in UAV images. *Computers and Electronics in Agriculture* 155:237–243

[22] Sankey TT. 2025. UAV hyperspectral-thermal-lidar fusion in phenotyping: genetic trait differences among Fremont cottonwood populations. *Landscape Ecology* 40:45

[23] Gu Y, Wang Y, Wu Y, Warner TA, Guo T, et al. 2024. Novel 3D photosynthetic traits derived from the fusion of UAV LiDAR point cloud and multispectral imagery in wheat. *Remote Sensing of Environment* 311:114244

[24] Zhang W, Qi J, Wan P, Wang H, Xie D, et al. 2016. An easy-to-use airborne LiDAR data filtering method based on cloth simulation. *Remote Sensing* 8:501

[25] Zhang J, Wang J, Dong P, Ma W, Liu Y, et al. 2022. Tree stem extraction from TLS point-cloud data of natural forests based on geometric features and DBSCAN. *Geocarto International* 37:10392–10406

[26] Fu H, Li H, Dong Y, Xu F, Chen F. 2022. Segmenting individual tree from TLS point clouds using improved DBSCAN. *Forests* 13:566

[27] Gao J, Tang L, Su H, Chen J, Yuan Y. 2025. Extraction of tree branch skeletons from terrestrial LiDAR point clouds. *Ecological Informatics* 85:102960

[28] Hartley RJL, Jayathunga S, Morgenroth J, Pearse GD. 2024. Tree branch characterisation from point clouds: a comprehensive review. *Current Forestry Reports* 10:360–385

[29] Wang K, Pu X, Li B. 2024. Automated phenotypic trait extraction for rice plant using terrestrial laser scanning data. *Sensors* 24:4322

[30] Li L, Mu X, Qi J, Pisek J, Roosjen P, et al. 2021. Characterizing reflectance anisotropy of background soil in open-canopy plantations using UAV-based multiangular images. *ISPRS Journal of Photogrammetry and Remote Sensing* 177:263–278

[31] Srinivasan S, Popescu S, Eriksson M, Sheridan R, Ku NW. 2015. Terrestrial laser scanning as an effective tool to retrieve tree level height, crown width, and stem diameter. *Remote Sensing* 7:1877–1896

[32] Liu F, Song Q, Zhao J, Mao L, Bu H, et al. 2021. Canopy occupation volume as an indicator of canopy photosynthetic capacity. *New Phytologist* 232:941–956

[33] Xu B, Wan X, Yang H, Feng H, Fu Y, et al. 2023. TIPS: a three-dimensional phenotypic measurement system for individual maize tassel based on TreeQSM. *Computers and Electronics in Agriculture* 212:108150

[34] Ustin SL, Gitelson AA, Jacquemoud S, Schaepman M, Asner GP, et al. 2009. Retrieval of foliar information about plant pigment systems from high resolution spectroscopy. *Remote Sensing of Environment* 113:S67–S77

[35] Gitelson A, Merzlyak MN. 1994. Quantitative estimation of chlorophyll-a using reflectance spectra: experiments with autumn chestnut and maple leaves. *Journal of Photochemistry and Photobiology B: Biology* 22:247–252

[36] Gitelson AA, Kaufman YJ, Merzlyak MN. 1996. Use of a green channel in remote sensing of global vegetation from EOS-MODIS. *Remote Sensing of Environment* 58:289–298

[37] Gitelson AA. 2004. Wide dynamic range vegetation index for remote quantification of biophysical characteristics of vegetation. *Journal of Plant Physiology* 161:165–173

[38] Gitelson AA, Kaufman YJ, Stark R, Rundquist D. 2002. Novel algorithms for remote estimation of vegetation fraction. *Remote Sensing of Environment* 80:76–87

[39] Gamon JA, Surfus JS. 1999. Assessing leaf pigment content and activity with a reflectometer. *New Phytologist* 143:105–117

[40] Thiel D, Kreyling J, Backhaus S, Beierkuhnlein C, Buhk C, et al. 2014. Different reactions of central and marginal provenances of Fagus sylvatica to experimental drought. *European Journal of Forest Research* 133:247–260

[41] Sims DA, Gamon JA. 2002. Relationships between leaf pigment content and spectral reflectance across a wide range of species, leaf structures and developmental stages. *Remote Sensing of Environment* 81:337–354

[42] An N, Welch SM, Cody Markelz RJ, Baker RL, Palmer CM, et al. 2017. Quantifying time-series of leaf morphology using 2D and 3D photogrammetry methods for high-throughput plant phenotyping. *Computers and Electronics in Agriculture* 135:222–232

[43] Liao L, Cao L, Xie Y, Luo J, Wang G. 2022. Phenotypic traits extraction and genetic characteristics assessment of *Eucalyptus* trials based on UAV-borne LiDAR and RGB images. *Remote Sensing* 14:765

[44] Sinaga KP, Yang MS. 2020. Unsupervised K-means clustering algorithm. *IEEE Access* 8:80716–80727

[45] Lambeth CC. 1980. Juvenile-mature correlations in Pinaceae and implications for early selection. *Forest Science* 26:571–580

[46] Isik K, Kleinschmit J, Steiner W. 2010. Age–age correlations and early selection for height in a clonal genetic test of Norway spruce. *Forest Science* 56:212–221